Influence of gas type on the thermal efficiency of microwave plasmas for the sintering of metal powders

Aidan Breen, Vladimir Milosavljević, Denis P. Dowling

[1]School Mechanical and Materials Engineering, University College Dublin, Belfield, Dublin 4, Ireland
(e-mail: denis.dowling@ucd.ie)
[2]Dublin City University, National Centre of Plasma Science and Technology, Collins Avenue, Glasnevin, Dublin 9, Dublin, Ireland

Abstract

Microwave plasmas have enormous potential as a rapid and energy efficient sintering technology. This paper evaluates the influence of both plasma atmosphere and metal powder type on the sintering temperatures achieved and the properties of the sintered powder metal compacts. The sintering is carried out using a 2.45 GHz microwave-plasma process called rapid discharge sintering (RDS). The sintering of three types of metal powder are evaluated in this study: nickel (Ni), copper (Cu) and 316L stainless steel (SS). An in-depth study of the effects of the plasma processing parameters on the sintered powder compacts are investigated. These parameters are correlated with the mechanical performance of the sintered compacts to help understand the effect of the plasma heating process. The substrate materials are sintered in four different gas discharges, namely hydrogen, nitrogen oxygen and argon. Thermocouple, pyrometer and emission spectroscopy measurements were taken to determine the substrate and the discharge temperatures. The morphology and structure were examined using scanning electron microscopy and x-ray diffraction. The density and hardness of the sintered compacts were correlated with the plasma processing conditions. As expected higher densities were obtained with powders with lower sintering temperatures i.e. nickel and copper when compared with stainless steel. Under the power input and pressure conditions used the highest substrate temperature attained was $1100^{\circ}C$ for Cu powder sintered in a nitrogen atmosphere. In contrast under the same processing conditions but in an argon plasma, the temperature achieved with SS was only $500^{\circ}C$. The effect of the plasma gas type on the sintered powder compact chemistry was also monitored, both hydrogen and nitrogen yielded a reducing effect for the metal in contrast with the oxidising effect observed in an oxygen plasma.

Key words: Microwave plasma, sintering, thermal measurements, emission spectroscopy

1 Introduction

The thermal sintering of metal powders has been widely reported using both furnace [1] and non-plasma microwave [2] treatments. Microwave sintering differs from conventional furnace techniques as the heating mechanism is volumetric rather than convective heating and decreased processing times are reported when compared with conventional heat treatment methods [3]. It is reported that powders sintered using microwaves exhibit more rounded powder particle porosity [4] and higher shrinkage rates [5] when compared with furnace sintering. In order to reach the elevated temperatures required to sinter materials with higher melting points, an alternative heating technique is required to microwave heating. The use of plasma treatments such as radio frequency [6] and DC sources [7] both

exhibit considerable potential in this regard as they offer a more homogeneous localised treatment for the sintering of metal powders. The microwave plasma technique has also been shown to exhibit considerable potential [8] and we have previously described the sintering process as rapid discharge sintering (RDS) [9]. During the RDS process gas molecules become excited by the microwaves and a plasma is formed, this in turn heats the material placed inside a plasma ball. In an early paper in this area, it was proposed that the discharge may cause activation of the particle surfaces that results in concentrated heat effects and hence, in an *in situ* cleaning action of powder particles [10]. Amongst the advantages of microwave plasmas is that they do not require susceptor heating and benefits from a cold wall processing technology, which means the cooling rate is very fast and power consumption is relatively low.

The type of plasma gas has been shown to influence the heating efficiency of the microwave plasma, which in turn has an impact on the densification of the material being processed [10]. It is reported for example that in the case of microwave plasmas that discharge temperatures were found to increase when diatomic gases were used compared with the temperatures obtained with argon for example [6]. Studies have shown that argon cannot reach sufficient sintering temperatures due to the lower enthalpy when compared with the diatomic gases [11]. The emission spectroscopy technique has been widely used to monitor the gas temperature in microwave plasmas [12]. As well as rotational gas temperature measurements for atmospheric plasma sources [13, 14]. Different gas species have also been investigated for spectral lines and emission characteristics, such as hydrogen H_2, nitrogen N_2 and oxygen O_2 as well as OH spectral lines [15, 16, 17].

This paper aims to systematically evaluate for the first time, the influence of both plasma gas type and powder type on the efficiency of the microwave plasma sintering process. The temperature of both the microwave plasma treated substrates and microwave plasmas themselves are monitored with changes in discharge gas and metal powder type.

2 Experimental Methods

Rapid Discharge Sintering process was carried out using a circumferential antenna plasma (CAP) as described in detail previously [9, 18]. The system shown in figure **Error! Reference source not found.** operates at 2.45 *GHz* with a 6 *kW* microwave power supply. The process required a 5 minute ramp up, a 10 minute treatment at the maximum temperature followed by a 5 minute cool down time, which gave a total processing time of 20 minutes

In this study the power input used for all experiments was 2.4 *kW* at a treatment pressure of 2 *kPa*. The four different discharge gases investigated to sinter the powder compacts were; Hydrogen, Oxygen, Argon and Nitrogen. In the case of H_2, N_2 and EO_2, a trace amount of Argon (Ar) was added to the main gas in order to facilitate actinometry measurements [15]. A gas flowrate of 100 *sccm* was used and 5 *sccm* flow of Argon for each study.

The plasma treatment experiments were carried out with three metal powders, these were; 1 μ*m* INCO ® nickel (T110) powder, 1 μ*m* Accu Powder® copper powder and 15-20 μ*m* Sandvik® 316L stainless steel powder. These powders were selected due to their relatively broad range of densities and melting points as detailed in Table 1.

Table 1: Melting point and bulk density of the powder metals investigated [19]

Powder	Melting Point ($^{\circ}C$)	Density (g/cm^3)
Copper (Cu)	≈1080	8.94
Nickel (Ni)	≈1450	8.90
Stainless Steel (SS)	≈1400	7.99

The powder compacts were pressed using a uniaxial 12.8 mm diameter die at a pressure of 600 *MPa*. The pressed "green" compact height was 10 *mm*. The dimensions of each sample were calculated based on the density of the powder and the packing density, to achieve equal sample sizes across the three powders. In each case both pressed and sintered cylinder densities were determined using Archimedes's principle. An photograph of the pressed compacts is shown in figure **Error! Reference source not found.**.

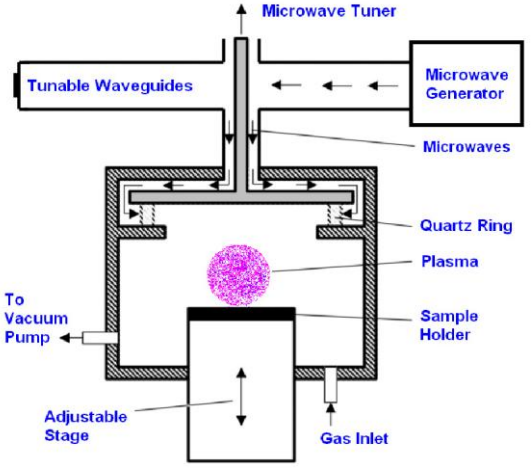

Fig. 1 Schematic of the circumferential microwave plasma rapid discharge sintering system

The pressed compacts were drilled before sintering using a 2.5 *mm* drill to a depth of approximately 4 *mm*, in order to accommodate the tip of an L-shaped S-type thermocouple, shielded in ceramic. The tip was inserted into the back of the vertical side of the sample and this facilitated *in situ* temperature measurement during sintering. The thermocouple was sourced from Industrial Temperature Sensors Ltd, with an upper limit of 1500 $^{\circ}C$. The surface temperature of the powder compacts were measured using a LASCON QP003 two–colour pyrometer (Dr. Merganthaler GmBH & Co, Ulm, Germany). The use of a two-colour pyrometer is expected to eliminate the interference effect of the plasma on the emissivity of the sample as no significant plasma emissions are observed for the gases used at the operating wavelengths of the pyrometer (1.68 and 1.916 μm) [20]. Substrate temperatures were obtained using light measurements through a quartz chamber window (approximately 40 mm in diameter). A temperature profile of the heating effect of the plasma was recorded for each compact tested.

Fig. 2 Image of the pressed Ni, Cu and SS samples before sintering

Optical emission spectroscopy was carried out using a low resolution spectrometer USB4000 UV/VIS with a spectral range of 200–880 *nm*. The emission spectra of each gas type was measured during the sintering of each of the metal powders and gases, to obtain the rotational and vibrational temperatures of the plasma species. Measurements were recorded at minute intervals, for the ten minute sintering process at the maximum treatment temperature. The gas temperature as determined using emission spectroscopy was compared with thermocouple and pyrometer readings recorded during the same tests. Argon was used as the actinometer to determinate relative atomic hydrogen and oxygen concentration, as well relative molecular nitrogen concentration [21, 22]. The selected actinometry lines are: argon at 750 *nm*, oxygen at 777 *nm*, hydrogen at 656 *nm* and molecular nitrogen 337 *nm*. For plasmas with hydrogen as a buffer gas, the rotational temperature of excited electron energy levels is determined from Fulcher-α diagonal bands ($d^3\Pi_u^- - a^3\Sigma_g^+$ electronic transition, P, Q and R branches), which were later used to derive rotation-vibration temperature of the hydrogen molecule ground state, which is assumed equal to gas temperature [23]. In the case of N_2 plasmas the plasma activated gas temperatures were deduced from the rotational temperature of nitrogen molecules emission of the second positive system i.e. N_2 $C^3\Pi_u^+ - B^3\Pi_g^+$. The corresponding vibrational band heads, $\mu = 0 = \mu' = 0, 1, 2, 3$ are located at the wavelengths, $\lambda = 337, 358, 380$, and 406 nm, respectively [24].

The density of both the green and sintered powder compacts was obtained using the Archimedes principle. The apparent density was found based on the Archimedes results and verified with the volume and mass measurements. Hardness tests were carried out on sintered compacts after they were mounted an polished. The Rockwell B hardness tests were carried out on the samples using a 1/16" steel ball and 100 *Kg* weight. SEM images were taken using a Hitachi TM–1000 scanning electron microscope to examine the polished surfaces and to determine the level of densification and particle necking after sintering. X–ray diffraction (XRD) was carried out on each sintered sample to determine the oxidation and sintered materials after processing. XRD analysis was carried out using a Siemens D500 XRD system over a scanning range of 20-80° with a step size of 0.02° and time per step of 1 *s*.

3 Results and discussion

3.1 Temperature Measurement

The thermal profile measurements with RDS heating obtained with a thermocouple and a two colour pyrometer are given in figure **Error! Reference source not found.**. As outlied earlier the thermocouple measurements were obtained using a probe inserted inside the compact while the pyrometer measurements are obtained at the surface of the powder compacts. The pyrometer system however can only measure temperatures above 546 $^{\circ}C$. There is a relatively close correlation between both the pyrometer and thermocouple readings, however there is an offset in that the pyrometer reading are approximately 20 $^{\circ}C$ lower than the thermocouple. This may be due to the focal area of the pyrometer, which can detect a large area both on the surface and the surrounding colder regions, which may lead to a small reduction in the recorded temperatures. Overall a balance between the volumetric heating of the microwaves and the convective heating associated with the plasma would lead to an overall homogeneous heating profile, as illustrated by the combined thermocouple and pyrometer readings [9, 25].

The thermocouple plots for each of the four gas types and the three types of metal powder are given in figure **Error! Reference source not found.**. These profiles demonstrate that the plasmas formed with H_2 and N_2 gases achieve the highest temperatures of approximately 1000-1100$^{\circ}C$ across all three materials, while plasmas formed with O_2 and Ar produce lower overall temperatures in the range of 500-700$^{\circ}C$. As outlined in the introduction section, these results confirm the observation reported previously that Ar produces a lower temperature due to the lower enthalpy compared with H_2 and N_2 gases [10, 6, 11]. The lower temperature observed in the case of the plasmas formed with O_2 is likely to be as a result of O_2 being the most electonegative of the three gases, with a tendency to create negative ions. These can cause a reduction in electron denstiy and would reflect in the plasma gas temperature when compared with H_2 and N_2 gases [26].

From figure **Error! Reference source not found.** it is clear that the thermocouple measurements obtained for both Cu and Ni were similar for the four gases evaluated. In contrast the temperature recorded in the case of SS was approximately 50$^{\circ}C$ lower for each of these gases. A possible explanation for this is that Cu and Ni both exhibit higher thermal conductivity and lowest electrical resistivity compared with SS. In the case of Cu the conductivity is 6 x10^7 Sm^{-1} , while that for Ni is 1.4 x10^7 Sm^{-1} and the value for SS is considerably lower at 1.5 x10^6 Sm^{-1} [27]. In the case of electrical resistivity the value for Cu and Ni is 2 x10^{-8} and 7 x10^{-8} Ωm respectively, while that for SS is 7 x10^{-7} Ωm [28]. In order to verify the the thermal results obtained with the powder compacts cylindrical bulk metals of the same materials (1 mm thick, x mm diameter), were heated in the plasma under the same processing conditions. The objective was to determine what maximum temperature could be achieved. These results are presented in figure **Error! Reference source not found.**. It can be seen that the Cu samples have the most rapid

heating rate and also the highest temperature obtained. The Ni show slightly lower thermal measurements while the maximum temperature obtained with SS (316L) of xxºC was x ºC lower than obtained with Cu.

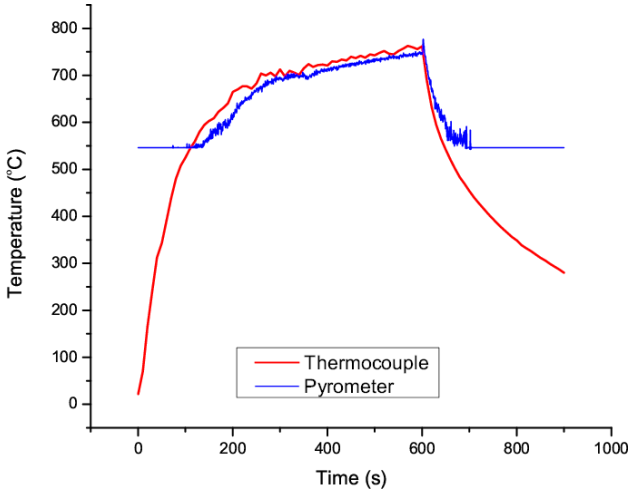

Fig. 3 Thermocouple and pyrometer measurements for copper compacts sintered in an O_2 plasma

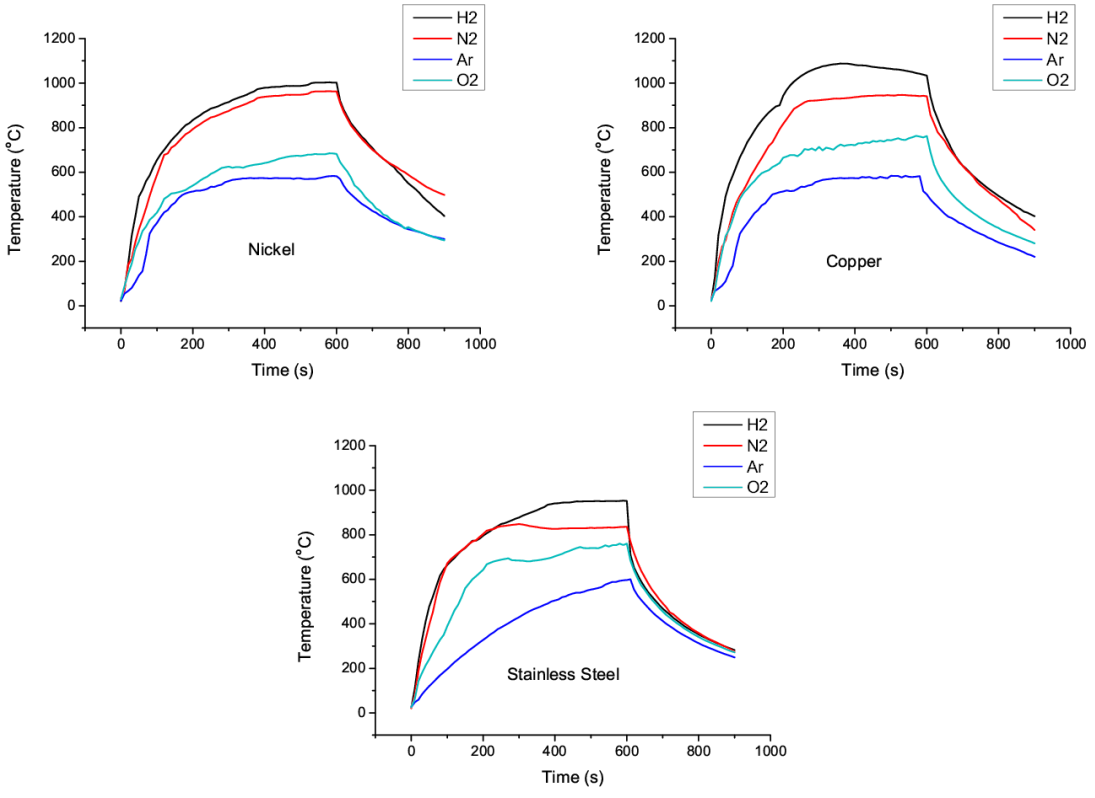

Fig. 4 Thermocouple measurements for nickel and copper and stainless steel compacts immersed in the microwave plasma formed using the gases shown. These figures demonstrates the rapid heating effect of the plasma and subsequent cooling once the plasma was turned off.

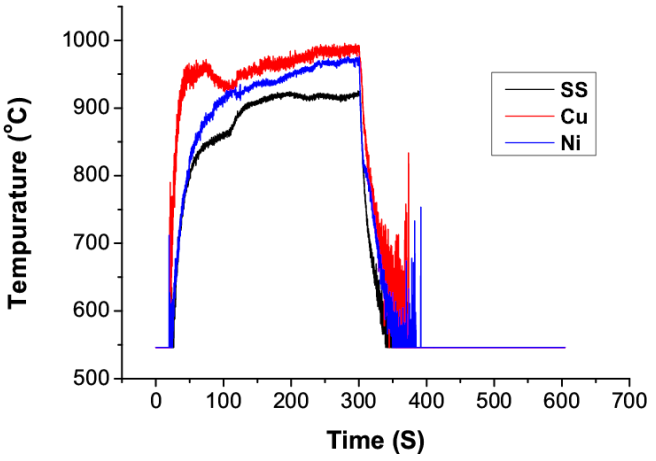

Fig. 5 Thermal profiles obtained with Cu, Ni and SS bulk material samples treated in the microwave plasma showing the different heating rates and thermal maxima obtained for each metal

3.1.1 Emission spectroscopy

The OES technique provides plasma diagnostic information on the rotational, vibrational and gas temperatures including the excitation temperature of certain group of excited levels [29, 30]. In the case of hydrogen plasmas, the rotational temperature of excited electron energy levels is determined from the Boltzmann plot of intensities of rotational molecular hydrogen lines belonging to Fulcher-α diagonal bands ($d^3\Pi_u^- - a^3\Sigma_g^+$ electronic transition; P, Q and R branches). In many publications [31, 23] the Fulcher-α band spectroscopy was used because of its strong visible emission intensity and few perturbations. The excitation energy from the ground state for the Fulcher-α system is 13.87 eV [31]. In this work emissions from the Q-branches of the $d^3\Pi_u$ state are used. The spectrometer used has a relatively low resolution therefore the spectral line recordings were performed with an instrumental profile very close to Gaussian form. To recover the true intensity of spectral lines of P, Q and R branches the multi-gaussian deconvoluting procedure has been applied [32]. Determination of rotation temperature is based the Boltzmann plot technique, which is widely used for rough estimation of rotation and vibrational temperature or rotation and vibrational population distribution, although the population density distribution over vibrational/rotation levels in gas discharge plasmas could be non-Boltzmann character as well [33, 34]. For the treatment of Ni, Cu and SS samples in a N_2 plasma, the rotational temperatures in the discharge were determined from the emission of nitrogen molecules. Emission bands of the second positive system of molecular nitrogen N_2 ($C^3\Pi_u^+ - B^3\Pi_g^+$) and the corresponding vibrational band heads, v = 0 =v'= 0, 1, 2, 3 are located at the wavelengths, λ = 337, 358, 380, and 406 nm, respectively have been used for temperature measurement. The method is based on fitting a tail of emission to the measurement points. Like in the case of hydrogen, it is considered that the population distribution among rotational sub-levels of molecular nitrogen is closely coupled to the translational energy distribution of the gas. Therefore it can be assumed that the rotational temperature is close to the kinetic gas temperature. In this experiment the mean rotational temperatures were calculated using the emission of each vibration band. The nitrogen second

positive system ($C^3\Pi_u^+ - B^3\Pi_g^+$) has been found to be free from overlap with other spectral features and the small quantum numbers of the states means that their population distribution is likely to be closer to equilibrium. The example of an N_2 emission spectrum is given in Figure **Error! Reference source not found.**.

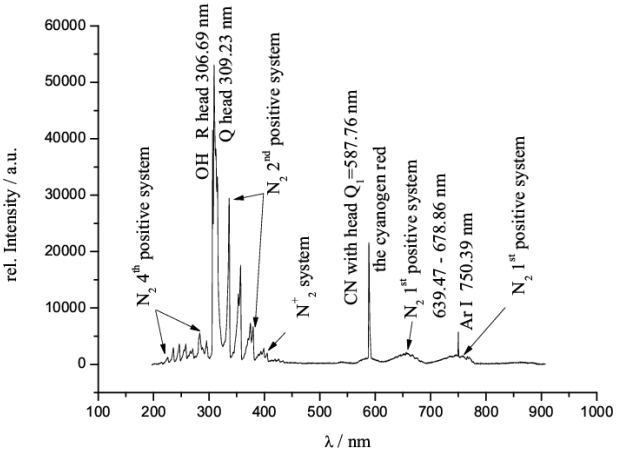

Fig. 6 Overall emission spectrum including the emission spectra of rotational lines for N_2 second positive system ($C^3\Pi_u^+ - B^3\Pi_g^+$). Experiment: nickel sample No.10 in mixture of N_2 (95%) and Ar (5%) at P= 2 kPa.

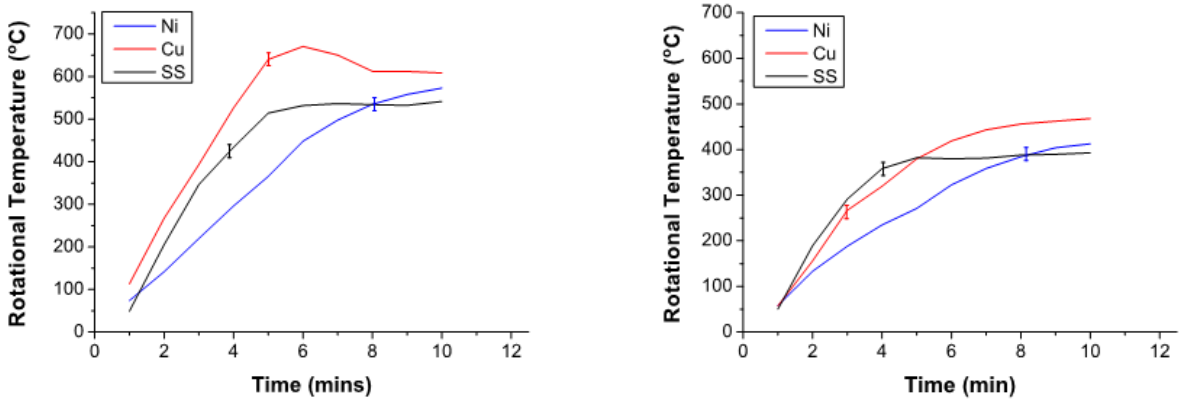

Fig. 7 The average rotational temperatures obtained for H_2 (left) and N_2 (right) during the plasma processing of Cu, Ni and SS powder compacts. 5% Ar was added as an actinometer to each discharge gas. The error bars on the graphs of each powder type (only one shown / graph), help demonstrate the relatively small fluctuation in the temperature measuremens for each of the different samples during sintering.

The results of temperature measurements for H_2 and N_2 plasmas is presented in Figure **Error! Reference source not found.** for discharges formed over each of the three substrates studied. . Note as detailed previously 5% of Ar have been added into the H2 and N2 discharges for actinometry measurements. The 750 nm Ar I spectral line was used for the actinometry experiments [35]. It has been shown previously that addition of up to 5% argon does not

significantly perturb the emission spectrum [21]. It has been shown that the temporal dependence of discharges and the presence of metastables can influence the time averaged rotational temperature of the molecules [36]. In our experiment we have very small amount of argon (5%). In this study the following emission of vibrational band heads were used, v = 0 =v'= 0, 1, 2, 3, located at the wavelengths, λ = 337, 358, 380, and 406 nm, respectively, which have been used for averaging a rotational temperature measurement. The temperature results were also checked with the (0 → 0) emission band of the first negative system of molecular nitrogen ions N_2^+ ($B^2\Sigma_u^+ - X^2\Sigma_g^+$) at 391 nm. Similar dependencies, for molecular nitrogen were found during the processing time.

As demonstrated in Figure **Error! Reference source not found.** under the power and processing conditions used the rotational temperature was generally found to increase with the sample processing time and then to stabilise. The temperature was found to be higher for the discharges formed over the Cu substrates than for obtained over Ni and SS. Overall, the rotational temperatures are in the range from 50 to 500 $^{\circ}C$. The rotational energy distribution is usually assumed to be in equilibrium with gas molecule kinetic energy distribution and so the rotational temperature is seen to reflect the neutral gas temperature within the chamber. It can be useful to study the relative changes in the concentration of atomic species in the discharge, in this case the study was carried out with oxygen, hydrogen and nitrogen as demonstrated in Figure **Error! Reference source not found.** which illustrate the actinometry measurements carried out. The overall density of the species are in very good agreement with the gas temperature measurements. The lower relative density of O_2 when compared with H_2 and N_2 correlates with the lower temperature found earlier for the thermocouple and pyrometer readings.

The lowest gas temperature recorded was for the hydrogen plasma treatment of the SS substrate, at the same time the density of hydrogen atom is the highest for this experimental condition. The stainless steel is a relatively stable material and hydrogen has the lowest chemical interaction with it in contrast with the Cu and Ni samples, because of that the levels of H_2 recorded in the spectra remain higher throughout the processing time.

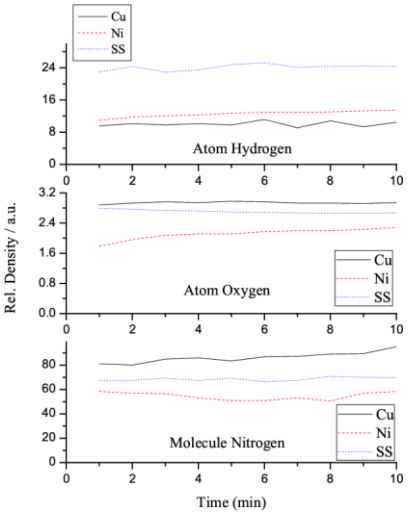

Fig. 8 Temporal evolution of the densities of the atomic oxygen, hydrogen and molecular nitrogen.

3.2 X-ray Diffraction

XRD analysis was carried out on all the powder compacts to evaluate their crystalline composition after sintering. As detailed in figure **Error! Reference source not found.** each powder behaved differently depending on the plasma treatment gas to which the powder was exposed. For samples sintered in an O_2 and Ar atmosphere, an oxide layer was formed on the surface of the materials. For SS samples sintered in N_2 and O_2, some α iron (ferrite) phase as well as some passivation with chromium oxide and iron oxide formation. The result of this XRD study is summarised as follows: From this study, it was concluded that:

- Oxidation occurred in both Ar and O_2 for all three powders compacts studied
- Cr_2O_3 and Fe_2O_3 were observed for SS sintered in the N_2 and O_2 plasmas
- No oxides were found in the reducing atmosphere of the H_2 plasma

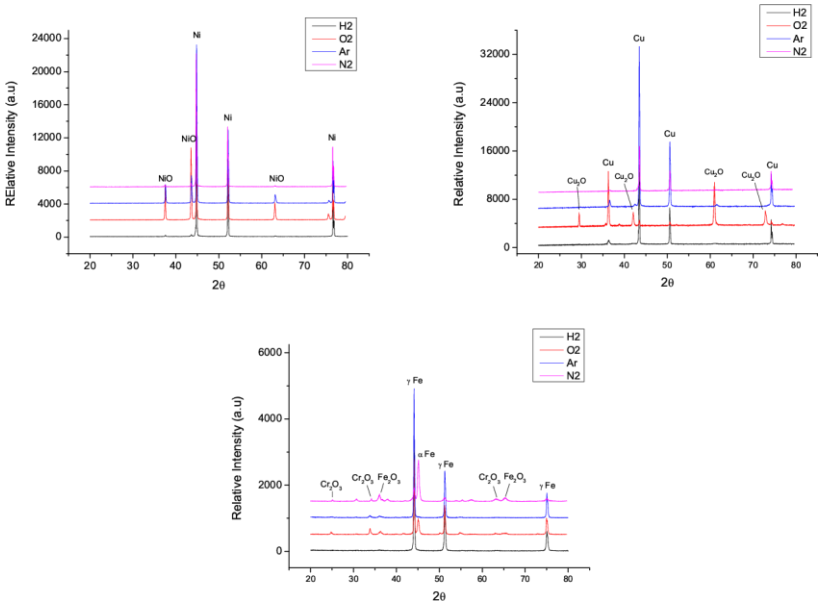

Fig. 9 XRD graphs of Ni, Cu and SS samples after sintering in each of the plasma gases shown

3.3 Density

Density measurements were recorded using Archimedes principle and volume measurements for each material before and after sintering. The average green density was found to be approximately 69% of theoretical density across all three material types. The bulk density values for Ni, Cu and SS are: 8.90, 8.94 and 7.99 g/cm^3 respectively [19]. The densities obtained for the sintered powder compacts are shown in figure **Error! Reference source not found.**. In each case it can be seen that higher densities are obtained for both copper and nickel compacts reflecting

their lower sintering temperatures. The H_2 and N_2 plasma treatments yielded compacts with the highest densities for all three powder types reflecting the higher temperatures achieved with these plasmas. The highest sintered densities achieved were 92 and 87% for the Ni and Cu samples respectively. while the SS samples reached a maximum density of 76%. The Cu compacts sintered in N_2 showed a large drop in density due to the high temperature of approximately 1100 $^{\circ}C$ reached during sintering. The melting point of the Cu compact was reached and thus the compact expanded during the solid to liquid transition, creating large pores and reducing the overall density of the sample after sintering.

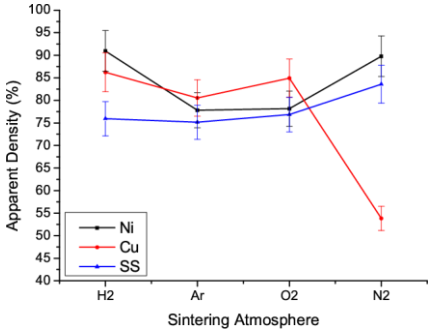

Fig. 10 Density measurements of the Ni, Cu and SS powder compacts after sintering in each of the plasma gases shown

3.4 Hardness

The hardness of each of the sintered compacts was measured using the Rockwell B indenter. As demonstrated in Figure **Error! Reference source not found.** the hardness values for each of the compacts correlated closely with the density measurements . SS with a bulk Rockwell hardness of approximately 90 HRB as expected exhibits a superior hardness value compared with Ni and Cu whose Rockwell values are 70 and 50 HRB respectively. The highest recorded hardness for the nickel and stainless steel samples was found to be 45.7 and 57.2 *HRB* respectively [37]. The variation in hardness of the individual compacts was relatively small in the case of Ni and SS for the four different plasma gases studied. In contrast in the case of Cu a very significant decrease in hardness is observed for the sample treated in the N_2 plasma due to melting. The results obtained for the hardness data in figure **Error! Reference source not found.** correlates directly with the density measurements given in figure **Error! Reference source not found.**.

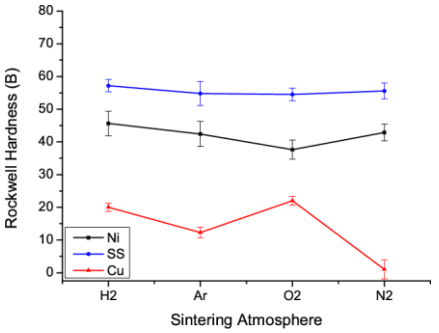

Fig. 11 Rockwell B Hardness measurements for nickel, copper and stainless steel sintered compacts

3.5 Morphology

The SEM images given in figure **Error! Reference source not found.** help to illustrate the differences in morphology in each powder metal compact sintered in a H_2 atmosphere. The stainless steel powers have a larger particle size (15-20 μm) and as a result the level necking between the particles is lower compared to that observed with the 1 μm copper and the nickel powder compacts. It has been shown previously that larger particles require a longer dwell time at the maximum temperature for increased necking and therefore higher densification to occur [1, 38].This would partially explain the higher level of porosity present in the sintered SS compact.

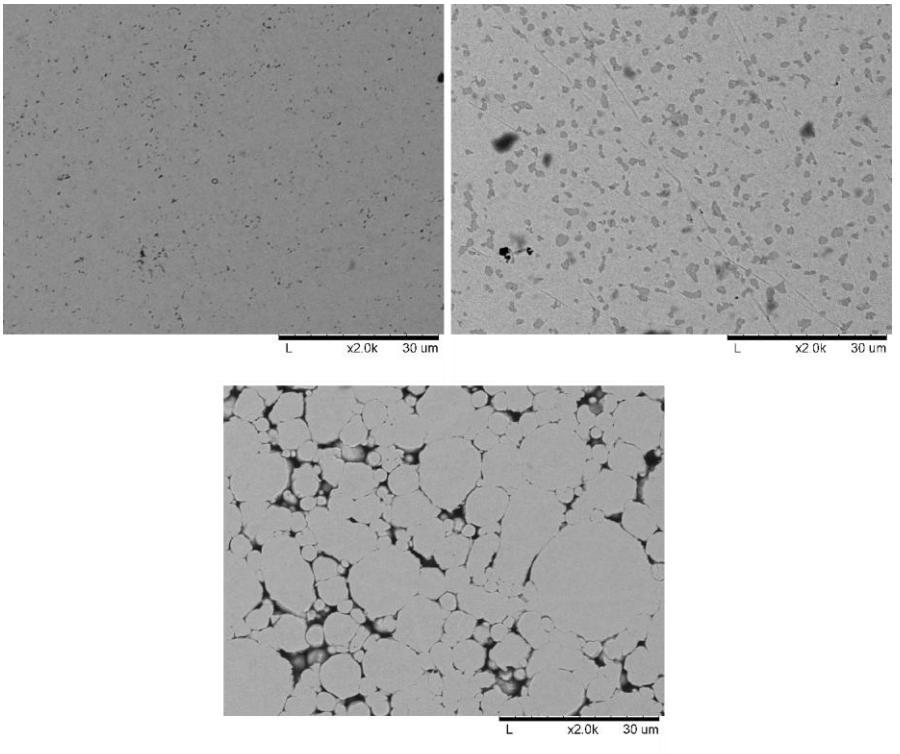

Fig. 12 SEM images of sintered Ni, Cu and SS taken at the center of each sample at 2000x magnification. The darker areas are associated with porosity.

4 Conclusions

The objective of this study was to systematically evaluate for the first time, the influence of both plasma gas type and powder type on the efficiency of the microwave plasma (Rapid discharge) sintering process. The following are the main conclusions from this study:

- The RDS thermal treatments were found to be reproducible and based on the examination of the morphology of sectioned samples, the heating effect appeared to be uniform across the 12 mm diameter compacts. The maximum recorded temperature using the thermocouple was 1100 $^{\circ}C$ for the copper and nickel compacts in a hydrogen plasma. The lowest temperature was 500 $^{\circ}C$ for samples treated in an argon atmosphere. For a given plasma gas type the heating effect of the plasma was found to be metal dependent which may be associated with the conductivity and resistance of the metal being treated.

- The OES analysis showed that the plasma gas temperature was lower than that obtained using the thermocouple and pyrometer methods, indicating that the plasma was being cooled on the outer section by the chamber walls and the central portion of the plasma ball had the most significant role in heating the powder compacts.

- The density of the sintered compacts was found to be dependent on both the metal type and plasma atmosphere used in the RDS treatment. The highest apparent density was 92% for the nickel samples treated in a hydrogen atmosphere. The copper samples reached their melting point when treated in a nitrogen plasma.

- The highest hardness for the nickel 45.7 *HRB* and 57.2 *HRB* for the stainless steel. The Cu was found to peak at 22 *HRB* when treated in an O_2 samples. The Ni and Cu compacts exhibited lower porosity than the steel compacts as the SS particles have not fully sintered at the temperatures reached in the RDS process.

- XRD data demonstrate that both oxidation and reduction of the powder compacts can be obtained depending on the gas used for the RDS treatments.

From this study it is concluded that the efficiency of plasma sintering is very dependent on the gas type used. In addition to sintering temperature however the oxidation / reduction effect of the plasma gas also has to be taken into consideration in the selection of the discharge gas for a specific powder compact.

Acknowledgements This work is part supported by Science Foundation Ireland 08/SRC/I1411. V. Milosavljevic is grateful to the Ministry of Science and Technological Development of the

Republic of Serbia (project No.171006).

References

[1] R. German, Metal Powder Industries Federation, USA (1994)

[2] D. Clark, W. Sutton, Annual Review of Materials Science **26**, 299 (1996)

[3] D. Agrawal, Current Opinion in Solid State and Materials Science **3**(5), 480 (1998)

[4] R. Wroe, Powder Metallurgy (Special Feature) pp. 24–28 (1999)

[5] K. Saitou, Scripta Materialia 54 pp. 875–879 (2006)

[6] D. Johnson, W. Sanderson, J. Knowlton, E. Demer, M. Chen, High Tech Ceramics.(Part A) pp. 815–820 (1986)

[7] J. LourenΓ§o, A. Maliska, A. Klein, J. Muzart, Materials Research **7**, 269 (2004)

[8] B. Twomey, A. Breen, G. Byrne, A. Hynes, D. Dowling, Metal Powder Report **65**(2), 10 (2010)

[9] B. Twomey, A. Breen, G. Byrne, A. Hynes, D. Dowling, Journal of Materials Processing Technology **211**(7), 1210 (2011)

[10] C. Bennett, N. McKinnon, L. Williams, Nature **217**, 1287 (1968)

[11] C. Chang, J. Szekely, J. Met. **34**(2), 57 (1982)

[12] X. Zhu, W. Chen, Y. Pu, Journal of Physics D: Applied Physics **41**, 105212 (2008)

[13] G. Nersisyan, W. Graham, Plasma Sources Science and Technology **13**, 582 (2004)

[14] V. Arkhipenko, A. Kirillov, L. Simonchik, S. Zgirouski, Plasma Sources Science and Technology **14**, 757 (2005)

[15] E. Bluem, S. Bechu, C. Boisse-Laporte, P. Leprince, J. Marec, Journal of Physics D: Applied Physics **28**, 1529 (1995)

[16] A. Ricard, P. Décomps, F. Massines, Surface and Coatings Technology **112**(1-3), 1 (1999)

[17] A. Ricard, M. Gaillard, V. Monna, A. Vesel, M. Mozetic, Surface and Coatings Technology **142**, 333 (2001)

[18] M. McConnell, D. Dowling, C. Pope, K. Donnelly, A. Ryder, G. O'Connor, Diamond and Related Materials **11**(3-6), 1036 (2002)

[19] P. Lee, *ASM Handbook Vol. 7, Powder Metal Technologies and Applications*, vol. 7 (1998)

[20] Y. Ralchenko, A. Kramida, J. Reader, N. Team, National Institute of Standards and Technology, Gaithersburg, MD (2008)

[21] J. Coburn, M. Chen, Journal of applied physics **51**(6), 3134 (1980)

[22] D. Popović, V. Milosavljević, S. Daniels, Journal of Applied Physics **102**, 103303 (2007)

[23] G. Majstorović, in *Journal of Physics: Conference Series*, vol. 133 (IOP Publishing, 2008), vol. 133, p. 012022

[24] U. Fantz, B. Heger, Plasma physics and controlled fusion **40**, 2023 (1998)

[25] A. Breen, B. Twomey, G. Byrne, D. Dowling, Materials Science Forum **672**, 289 (2011)

[26] C. Lee, D. Graves, M. Lieberman, D. Hess, Journal of the Electrochemical Society **141**, 1546 (1994)

[27] D. Griffiths, R. College, *Introduction to electrodynamics*, vol. 3 (prentice Hall New Jersey;, 1999)

[28] U. Ugur, Online: http://hypertextbook.com/facts/2006/UmranUgur.shtml (2011)

[29] J. Röpcke, M. Käning, B. Lavrov, Le Journal de Physique IV **8**(PR7) (1998)

[30] NIST - Atomic Spectra Data Base Lines (wavelength order), (2011)

[31] U. Fantz, Plasma physics and controlled fusion **40**, 1035 (1998)

[32] V. Milosavljević, G. Poparić, Phys. Rev. E **63**(3), 036404 (2001)

[33] G. Herzberg, (1950)

[34] J. Phillips, in *Optical Spectrometric Measurements of High Temperatures*, vol. 1 (1961), vol. 1, p. 217

[35] V. Milosavljević, R. Faulkner, H.M. B., Optics Express **15**(21), 13913 (2007)

[36] C. Nwankire, V. Law, A. Nindrayog, B. Twomey, K. Niemi, V. Milosavljević, W. Graham, D. Dowling, Plasma chemistry and plasma processing **30**(5), 537 (2010)

[37] AZOM. A to z of materials (2011). URL http://www.azom.com/

[38] K. Komeya, H. Inoue, Journal of Materials Science **4**(12), 1045 (1969)